ELSEVIER

Journal of Molecular Catalysis A: Chemical 163 (2000) 27–42

JOURNAL OF MOLECULAR CATALYSIS A: CHEMICAL

www.elsevier.com/locate/molcata

The effects of synthesis and pretreatment conditions on the bulk structure and surface properties of zirconia

Kyeong Taek Jung, Alexis T. Bell*

Chemical Sciences Division, Lawrence Berkeley National Laboratory and Department of Chemical Engineering, University of California, Berkeley, CA 94720-1462, USA

Received 7 March 2000; accepted 25 July 2000

Abstract

An investigation has been conducted to establish the effects of synthesis conditions and subsequent calcination conditions on the bulk and surface properties of zirconia. Samples of zirconia were prepared by precipitation from an aqueous solution of zirconyl chloride at both high and low pH. Precipitation at high pH (10) produced an amorphous material with a surface area of 280 m^2/g. Extended digestion of this material in a boiling NH_4OH solution at 1 atm increased the surface area to 400 m^2/g. When digestion was carried out at ~3 atm, the amorphous zirconia became crystalline and its surface area reduced to 200 m^2/g. Precipitation of zirconia at low pH (<1.5) with extended reflux produced monoclinic ZrO_2 with a surface area of 110 m^2/g. Calcination at temperatures in the range of 300–1200 K caused a loss in surface area with increasing temperature and induced the amorphous-tetragonal and tetragonal-to-monoclinic phase transformations. The surface concentration of hydroxyl groups on monoclinic ZrO_2 is always higher than that on tetragonal ZrO_2. In the former case the dominant species are tribridged hydroxyl groups and in the latter, a combination of bibridged and terminal hydroxyl groups. CO_2 adsorbs on zirconia at 298 K to form bicarbonate species and a smaller amount of carbonate species. The surface concentration of bicarbonate species grows monotonically with the surface concentration of hydroxyl groups. A similar relationship is observed for the adsorption of CO as formate species. Consistent with these results, monoclinic zirconia adsorbs more CO and CO_2 than tetragonal zirconia.

Keywords: ZrO_2; Bulk structure; HpHUT; HpHLP; HpHHP; LpHLP

1. Introduction

Zirconium oxide has attracted considerable attention recently as both a catalyst and a catalyst support because of its high thermal stability and the amphoteric character of its surface hydroxyl groups. Zirconia catalyzes the hydrogenation of olefins [1–4], isomerization of olefins [5] and epoxides [6,7], and the dehydration of alcohols [8,9]. When zirconia is used as a support, various reactions such as Fischer–Tropsch synthesis [10,11] methanol synthesis [12–15], and hydrodesulfurization [16] have been reported to proceed with higher activity and selectivity than with conventional supports.

The applications for zirconia described above have stimulated research aimed at understanding the factors controlling the structural and textural properties of ZrO_2, such as; the distribution of ZrO_2 among amorphous, tetragonal, and monoclinic phases; the BET surface area; and the pore size distribution

* Corresponding author. Tel.: +1-510-642-1536; fax: +1-510-642-4778.
E-mail address: bell@cchem.berkeley.edu (A.T. Bell).

1381-1169/00/$ – see front matter
PII: S1381-1169(00)00397-6

[17–29]. Studies have also been carried out to identify the relationships between bulk and surface properties of ZrO_2. Infrared spectroscopy has revealed the presence of three types of hydroxyl groups on ZrO_2: terminal, bibridged, and tribridged [30–38]. Using CO as the probe molecule, it has been established that Lewis-acidic sites, while more abundant on monoclinic ZrO_2, are not as strong as those on tetragonal ZrO_2 [38–46]. The adsorption of CO results in the appearance of molecularly adsorbed CO and formate species. The latter are formed as a consequence of the reaction of CO with hydroxyl groups on the surface of ZrO_2. Upon CO_2 adsorption on monoclinic ZrO_2, bicarbonate and monodentate and bidentate carbonates are formed, while bidentate and polydentate carbonates are formed on tetragonal ZrO_2 [39,40,47–51]. Monoclinic ZrO_2 is found to form stronger bonds with CO_2 than tetragonal ZrO_2 [51].

The present investigation was undertaken to establish the effects of synthesis conditions on the bulk structure and surface properties of ZrO_2. Zirconia was precipitated from zirconyl chloride solutions at both low and high pH, both with and without subsequent hydrothermal treatment. The freshly prepared material was then calcined in oxygen at progressively higher temperatures. The bulk structure was characterized by X-ray diffraction. The characteristics of the hydroxyl groups present at the surface of ZrO_2 were characterized by infrared spectroscopy. Both CO and CO_2 were used as probe molecules to further characterize the acidic and basic properties of ZrO_2.

2. Experimental

Four samples of zirconia were synthesized. The first was prepared by boiling a 0.5 M solution of zirconyl chloride ($ZrOCl_2{\cdot}8H_2O$, Aldrich) under reflux at 373 K and 1 atm for 240 h, while maintaining the pH at 1.5. This sample is designated as LpHLP (Low pH Low Pressure). The remaining three samples were prepared by dropwise addition of 30 wt.% ammonium hydroxide to a 0.5 M solution of zirconyl chloride at a constant pH of 10. The slurry of precipitated material was then divided into three batches. The first batch was left untreated in the presence of the mother liquor at 298 K for 240 h. This sample is designated as HpHUT (High pH Untreated). The second batch of precipitated material was heated in the mother liquor, after adjusting its pH to 10, at 373 K and 1 atm for 240 h. This sample is designated as HpHLP (High pH Low Pressure). The third batch of precipitate was transferred to a 23 cm^3, teflon lined autoclave and heated in an oven at 383 K and an autogenous pressure of ∼3 atm for 240 h. This sample is designated as HpHHP (High pH High Pressure). In all cases, the final product was recovered by vacuum filtration. The solid product was then redispersed in deionized water and washed in order to remove residual chlorine. After each wash, a few drops of $AgNO_3$ solution were added to the filtrate liquid until no evidence of AgCl could be detected. This usually required 50 washings with a total of 10 l of water. The washed product was then dried at 373 K in a vacuum oven for 24 h. The dried samples were then calcined in pure O_2 in a tube furnace. The temperature was increased from 298 K to the desired calcination temperature at the rate of 10 K/min and then held at the final temperature for 5 h.

X-ray diffraction (XRD) patterns of the dried and calcined samples were recorded using a Siemens D5000 diffractometer, which uses Cu-Kα radiation and a graphite monochrometer. Scans were made in the 2θ range of 10–70° at a scanning rate of 0.005°/s. The volume fraction, V_m, of monoclinic ZrO_2 (m-ZrO_2) was determined from the following relationships [52]:

$$X_m = \frac{I_m(1\,1\,1) + I_m(1\,1\,\bar{1})}{I_m(1\,1\,1) + I_m(1\,1\,\bar{1}) + I_t(1\,1\,1)} \quad (1)$$

$$V_m = \frac{1.311X_m}{1 + 0.311X_m} \quad (2)$$

where $I_m(1\,1\,1)$ and $I_m(1\,1\,\bar{1})$ are the line intensities of the (1 1 1) and (1 1 $\bar{1}$) peaks for m-ZrO_2, and $I_t(1\,1\,1)$ is the intensity of the (1 1 1) peak for tetragonal ZrO_2 (t-ZrO_2). The crystal size, d_{hkl}, was calculated from the Scherer relationship using the integral line width, B_{hkl}, for the monoclinic and tetragonal phases, following line deconvolution, and a shape factor, S, equal to 0.9.

An Autosorb gas adsorption system was used to obtain nitrogen adsorption/desorption isotherms at 77 K. Before analysis, each sample was evacuated at either 373 (uncalcined samples) or 523 K (calcined samples). The BET surface area was determined from an 80-point isotherm.

3. Results

3.1. Effects of preparation conditions on the bulk structure of ZrO_2

XRD patterns of the LpHLP, HpHUT, HpHLP, and HpHHP ZrO_2 are shown in Fig. 1a–d. The only features present in the diffraction pattern of LpHLP ZrO_2 are those characteristic of m-ZrO_2 (see Fig. 1a). With increasing calcination temperature, these features become sharper and better resolved, indicative of an increase in the size of the crystallite particles. As-prepared HpHUT ZrO_2 is completely amorphous up to a calcination temperature of 673 K, at which point peaks for crystalline t-ZrO_2 appear (see Fig. 1b). At higher calcination temperatures the intensity of the peaks for t-ZrO_2 decrease as peaks for m-ZrO_2 appear. HpHLP ZrO_2 is also amorphous in its as-prepared state and remains as such until the calcination temperature is raised to 873 K (see Fig. 1c). At this temperature broad peaks appear for t-ZrO_2, and these features become sharper as the temperature of calcination is raised further. As-prepared HpHHP ZrO_2 consists of mainly t-ZrO_2 with a small amount of m-ZrO_2 (see Fig. 1d). With increasing calcination temperature the relative intensity of the diffraction features for m-ZrO_2 increases, whereas those for t-ZrO_2 decrease.

Fig. 2 illustrates the effects of preparation method and calcination temperature on the distribution between t- and m-ZrO_2. Data points are plotted only for those samples that are completely crystalline. The volume fraction of m-ZrO_2 is a strong function of both the method of preparation and the calcination temperature. The HpHLP samples remain as t-ZrO_2 until the calcination temperature is raised above 1373 K, at which point the material is completely converted to m-ZrO_2. By contrast the LpHLP samples are always m-ZrO_2, independent of the calcination temperature. The HpHUT and HpHHP samples exhibit a mixture of t- and m-ZrO_2, the proportion of m-ZrO_2 increases with increasing calcination temperature.

The size of the particles of t- and m-ZrO_2, estimated from X-ray line broadening is shown in Fig. 3. The HpHLP method of preparation results in t-ZrO_2 crystallites, that have an average size of 5 nm at 973 K and increase to 15 nm as the temperature rises. When calcined at 1473 K, this material produces 21 nm particles of m-ZrO_2. Preparation of m-ZrO_2 via the LpHLP procedure leads to 4 nm particles that grow to 21 nm as the calcination temperatures rises from 473 to 1273 K. The HpHUT and HpHHP methods of preparation produce a mixture of t- and m-ZrO_2. For the untreated samples, the size of the t-ZrO_2 particles are larger than those of m-ZrO_2 for calcination temperatures less than 873 K, but the reverse becomes true at higher temperatures. A similar pattern is also observed for ZrO_2 prepared via the HpHHP method.

Fig. 4 shows the effects of sample preparation method and calcination temperature on the BET surface area. For calcination at 373 K, the highest surface area is observed for samples prepared by the HpHLP method, and the lowest surface area is observed for samples prepared by the LpHLP method. As the calcination temperature increases, the BET surface area decreases in all cases. Interestingly, the HpHUT, HpHHP, and HpHLP samples all approach the same surface area once the calcination temperature rises above about 673 K. This pattern is consistent with the change in particle size with increasing calcination temperature, shown in Fig. 3. There too, it is seen that the size of t-ZiO_2 particles remains much smaller than that of particles of either phase produced by other preparation methods.

The results presented in Figs. 1–4 demonstrate that the phase, surface area, and particle size of ZrO_2 produced is strongly dependent on the pH of the synthesis mixture and the conditions of thermal treatment following the initial formation of the solid. Calcination of the freshly prepared material can result in further changes in each of these properties. Both the effects of synthesis conditions and calcination temperature can be interpreted in the light of the literature concerning the synthesis of ZrO_2.

X-ray studies have shown that aqueous solutions of $ZrOCl_2{\cdot}8H_2O$ contain tetrameric $[Zr(OH)_2{\cdot}4H_2O]_4{}^{8+}$ cations [53]. The metal ions form a square and are bonded to each other by bridging hydroxyl groups. Each of the metal atoms is eight-coordinate with four molecules of water filling out the coordination sphere of the zirconium atoms. Boiling zirconyl chloride solutions causes the tetrameric cations to polymerize via hydroxyl bridging and eventual olation [19]. This process produces an amorphous hydrous zirconia with the general formula $[ZrO_x(OH)_{4-2x}\cdot yH_2O]_n$. At low pH (<2) the solubility of the amorphous material is appreciable. Repeated dissolution and precipitation

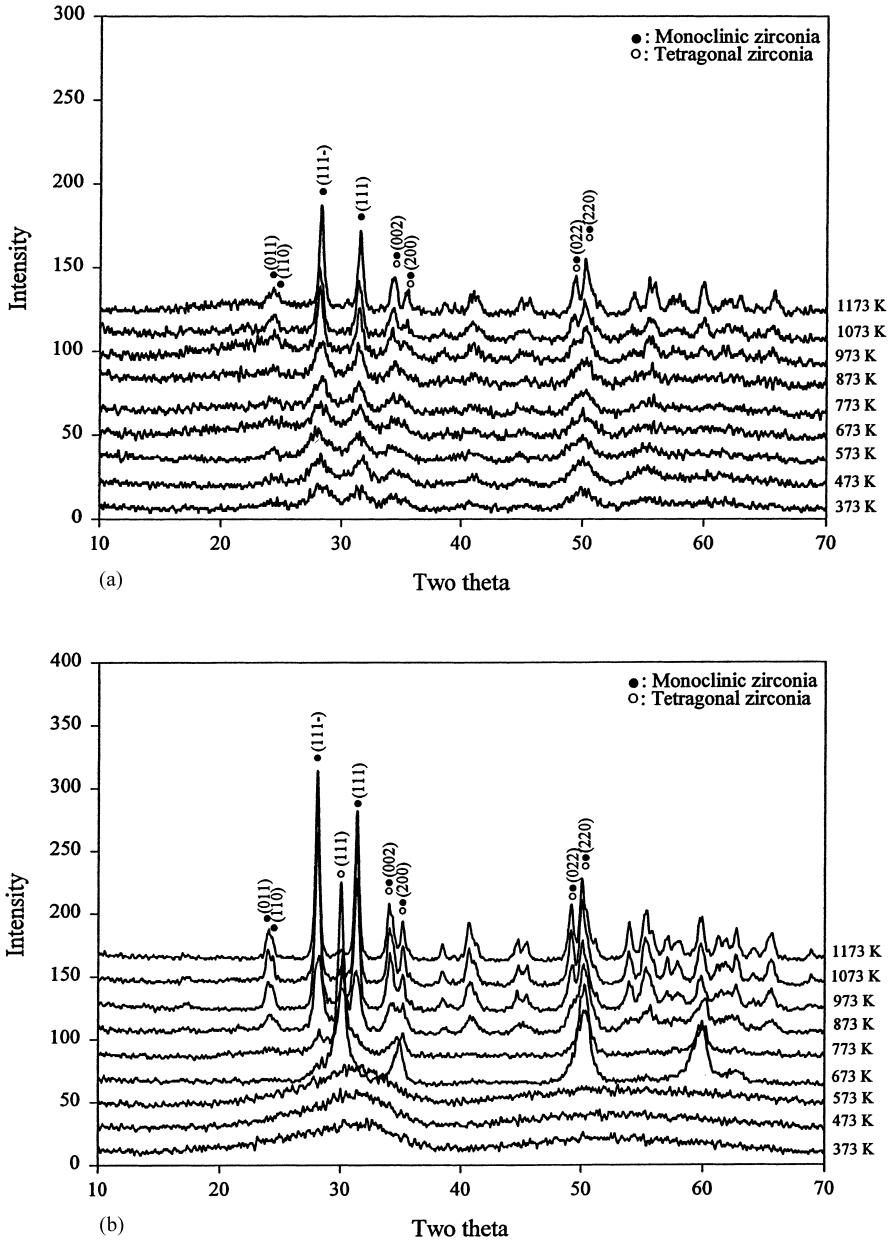

Fig. 1. Effect of calcination temperature on the X-ray diffraction patterns for samples prepared at (a) low pH and low pressure (LpHLP), (b) high pH and untreated (HpHUT), (c) high pH and low pressure (HpHLP), and (d) high pH and high pressure (HpHHP).

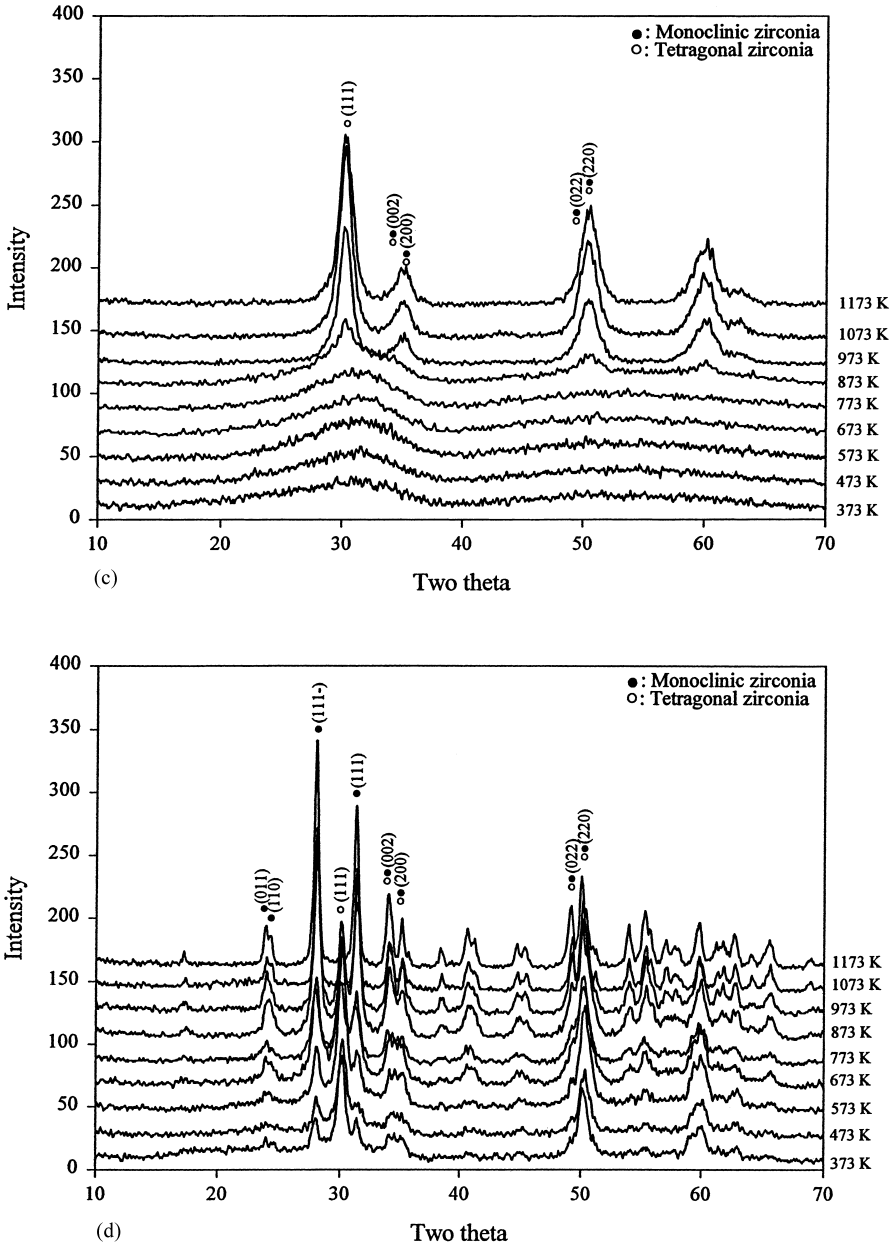

Fig. 1 (*Continued*).

leads to the formation of small (2.0–2.5 nm) particles of crystalline hydrous zirconia, which then rearrange to form crystallites of m-ZrO_2 [19]. Precipitation of amorphous hydrous zirconia at pH >3 at elevated temperatures tends to produce a more disordered and highly hydrated product than that formed at lower pH's. Dewatering of this material leads to the formation of crystalline t-ZrO_2.

Hydrothermal treatment at high pH (>9) causes the initially precipitated hydrous zirconia to undergo dissolution and reprecipitation. The reprecipitated material consists of particles that are smaller than those in

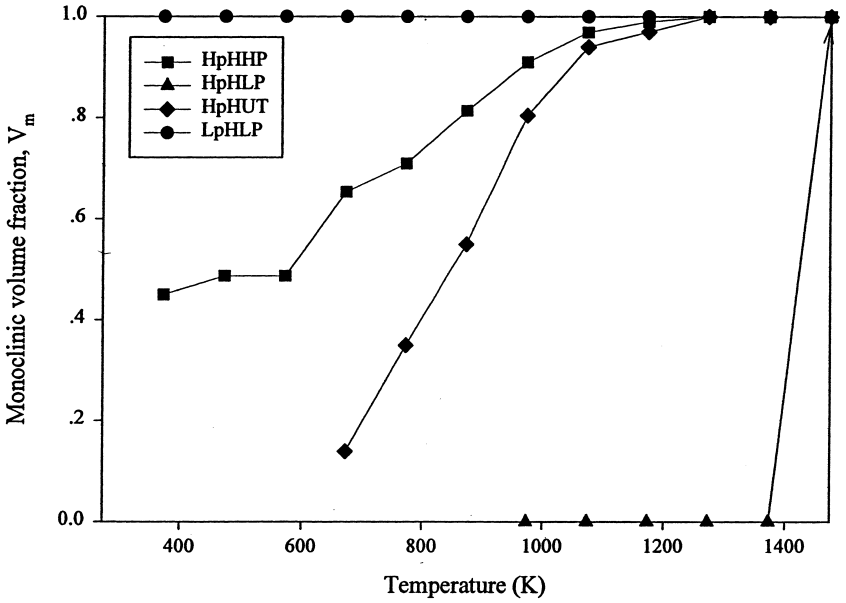

Fig. 2. Effect of preparation conditions on the volume fraction of monoclinic zirconia as a function of calcination temperature.

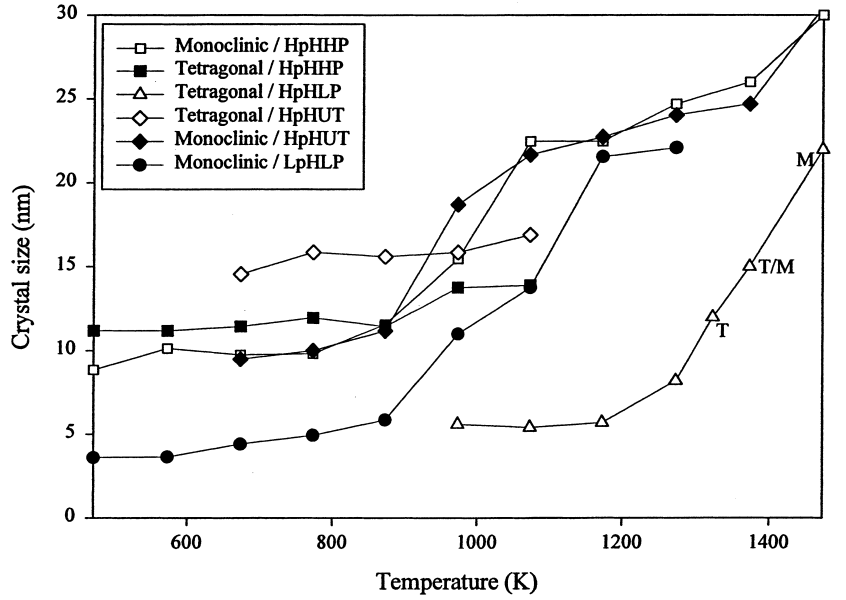

Fig. 3. Effect of preparation conditions and calcination temperature on the crystal size of tetetragonal and monoclinic zirconia.

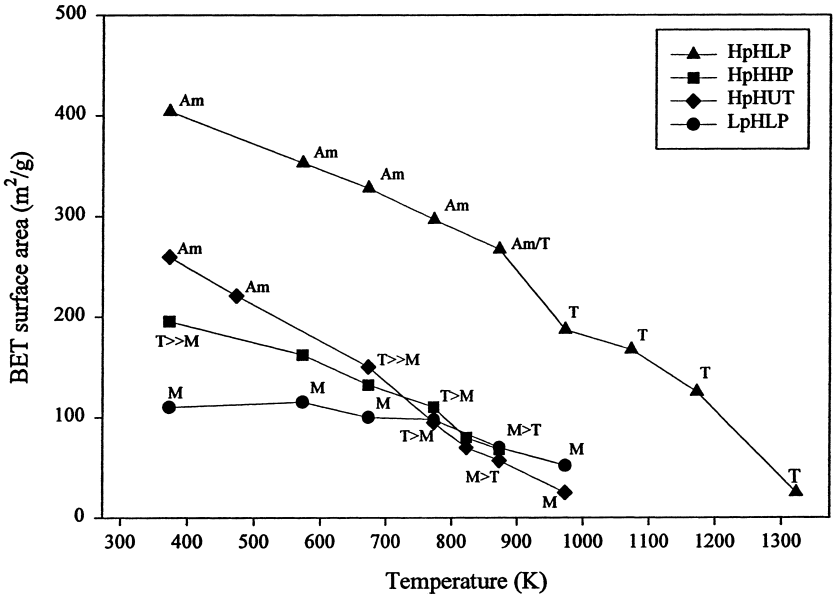

Fig. 4. Effect of preparation conditions and calcination temperature on the BET surface area of amorphous (Am), tetetragonal (T), and monoclinic (M) zirconia.

the initial precipitate. Adsorption of the cations of the base used to elevate the pH (e.g. Na^+, K^+, $NH_4{}^+$) helps to stabilize the surface area by neutralizing the negatively charged surface of the particles, allowing them to form a stable network [19]. Cation adsorption also favors the formation of the tetragonal phase of zirconia, the effect increasing in the order NH_4^+, $< K^+$, $< Na^+$.

The results presented here are consistent with the earlier studies cited above. The LpHLP sample prepared by precipitation zirconia from an aqueous solution of zirconyl chloride at pH <1.5 with extended reflux, results in the formation of m-ZrO_2 with a BET surface area of 110 m^2/g. By contrast, precipitation from a solution maintained at pH = 10 by addition of NH_4OH, the sample designated as HpHLP, followed by extended digestion in the mother liquor produces amorphous zirconia with a surface area of 400 m^2/g. If the precipitate produced at high pH is not allowed to undergo digestion, the sample designated as HpHUT, amorphous zirconia is obtained once again, but with a BET surface area of 280 m^2/g. Thus, it is apparent that extended digestion of the initial precipitate increases the surface area of the final product. Digestion of the high pH precipitate at elevated pressure (∼3 atm), the sample designated as HpHHP, induces crystallization of the initially amorphous precipitate and a small loss in BET surface area to 200 m^2/g. As discussed below, these effects are likely the result of the increased thermodynamic driving force resulting from the higher pressure at which digestion is carried out.

The data presented in Figs. 2 and 3 show that calcination of the initially prepared zirconia at progressively higher temperatures leads to the conversion of amorphous zirconia to t-ZrO_2 and the conversion of this phase to m-ZrO_2. The amorphous-to-tetragonal transformation is attributable to the loss of water from the amorphous hydrous zirconia, resulting from the release of water of hydration and the production of water via olation [19]. Both processes lead to a reduction in the BET surface area of the calcined solid and a consequent increase in the average particle size. Identification of the factors affecting the tetragonal-to-monoclinic transformation have been the subject of significant discussion in the literature [17–28]. It has been proposed that the relative stability of these two phases depends on the sum of the free energies from particle surface, bulk, and strain contributions [54–59]. Because of the lower bulk free energy of m-ZrO_2 and the lower surface free energy

Table 1
Sample preparation conditions of zirconia for TPD measurement and the concentration of hydroxyl groups

Crystalline phase	BET surface area (m^2/g)	Preparation method	Calcination temperature	OH concentration (molecule/nm^2)
Amorphous	325	HpHLP	673	2.1
	187	HpHLP	973	1.6
Tetragonal	20	HpHLP	1323	3.5
Monoclinic	110	LpHLP	573	9.4
	19	HpHUT	973	6.2
Tetragonal/Monoclinic	80	HpHHP	823	5.3

of t-ZrO_2, the latter phase is stabilized below a critical particle size for a given temperature. This critical particle size is estimated to be 10 nm at 298 K [58]. In the absence of particle strain, this thermodynamic description has been found to give the correct temperature for the tetragonal-to-monoclinic phase transformation for particles ranging in size from 9 nm to 10 μm [58]. The validity of a purely thermodynamic explanation has been questioned, though, since several investigators have observed t-ZrO_2 particles that are larger than the critical particle size, e.g. [17,18]. However, these observations can be explained by taking into account factors such as domain boundary stresses, nucleation embryos, anionic vacancies, and adsorbed cations and anions, all of which contribute to the stabilization of t-ZrO_2. Of these various factors, the effects of external strain and the adsorbed ionic species on the surface free energy of zirconia can be accommodated within the thermodynamic theory for the tetragonal-to-monoclinic phase transformation [58].

The thermodynamic theory for the tetragonal-to-monoclinic transformation of ZrO_2 leads to the conclusion that in the absence of strain, ZrO_2 particles with an average diameter 10 nm, should exist as m-ZrO_2 at 298 K. If it is assumed that the particles are hemispherical in shape, this means that sintering of ZrO_2 to a BET surface area of about 110 m^2/g will lead to its transformation to m-ZrO_2. Reference to Fig. 4 shows that with the exception of the HpHLP samples the data support this conclusion. The stability of t-ZrO_2 in the HpHLP samples to surface areas of 20 m^2/g suggests that the particles in these samples may be polycrystalline and strained [58]. A similar explanation would apply to the observation of t-ZrO_2 particles as large as 13 and 16 nm in the HpHUT and HpHHP samples, respectively, seen in Fig. 3.

3.2. Surface properties of ZrO_2

A series of ZrO_2 samples were selected to assess the effects of bulk structure on the surface properties of the ZrO_2 particles. Table 1 lists the phase composition of each sample, together with the BET surface area and the concentration of OH groups. The highest concentration of OH groups is observed for the sample of m-ZrO_2 having a surface area of 110 m^2/g, and the lowest is for sample of t-ZrO_2 having a surface area of 187 m^2/g. The concentration of OH groups on the surface of the sample of amorphous ZrO_2 is similar to that of the high surface area tetragonal ZrO_2 sample.

Not only the concentration, but also the nature of the OH groups present on ZrO_2 depends on the bulk phase structure and the BET surface area. Fig. 5 shows infrared spectra of the O–H stretching region. Three bands are observed at 3765, 3745, and 3650–3670 cm^{-1}. These features have been assigned to terminal, bibridged, and tribridged OH groups, respectively [31–35]. The distribufion of OH groups is illustrated by a bar graph presented in Fig. 6. The hydroxyl groups on t-ZrO_2 are predominantly bibridged, whereas those on m-ZrO_2 they are predominantly tribridged. Amorphous ZrO_2 has roughly equivalent numbers of all three types of groups, whereas the sample containing a 50/50 mixture of t- and m-ZrO_2 has an OH spectrum that is most similar to that of m-ZrO_2.

Curves showing the rate at which HD is produced when D_2 is passed over the surface of ZrO_2 while it is being heated are presented in Fig. 7. No evidence for desorption of H_2 or D_2 was observed in these experiments. The lowest peak temperature (473 K) for H/D exchange is observed for t-ZrO_2 (20), where the quantity in parenthesis indicates the BET surface area.

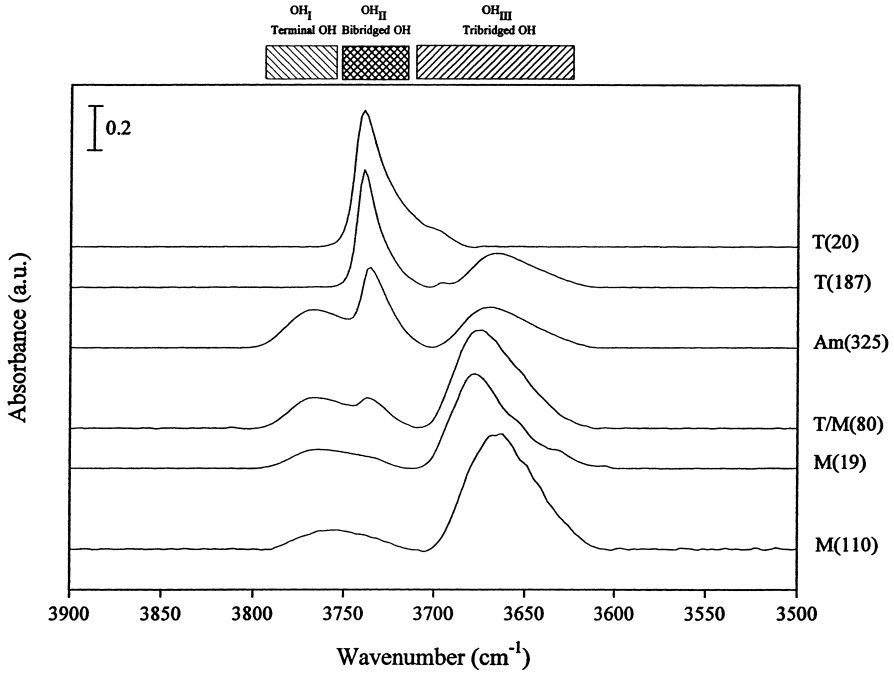

Fig. 5. Infrared spectra of the hydroxyl groups present on the surface of zirconia. Each sample is identified as X (*Y*), where X = Am, T, T/M, or M and *Y* designates the BET surface area in m^2/g.

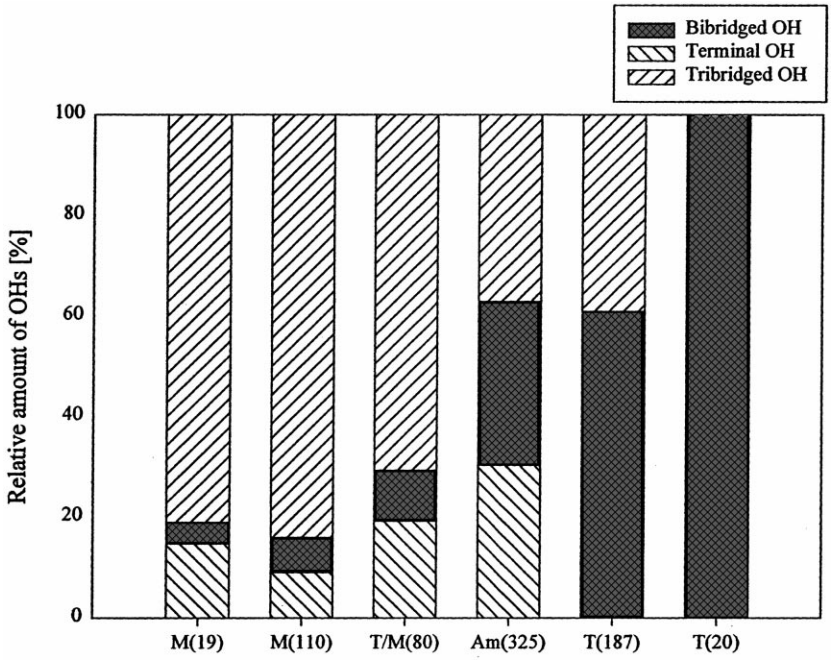

Fig. 6. The distribution of isolated, bibridged, and tribridged hydroxyl groups on the surface of zirconia. Each sample is identified as X (*Y*), where X = Am, T, T/M, or M and *Y* designates the BET surface area in m^2/g.

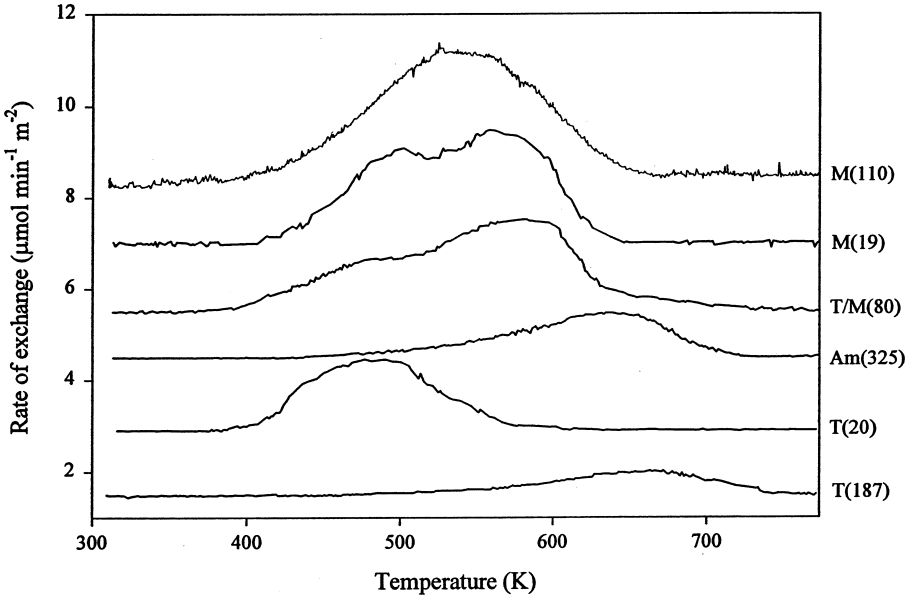

Fig. 7. Temperature-programmed isotopic exchange spectra. Each sample is identified as X (*Y*), where X = Am, T, T/M, or M and *Y* designates the BET surface area in m^2/g.

A similar peak is seen as a component of the H/D exchange spectra presented for m-ZrO_2 (110), m-ZrO_2 (187) and t-/m-ZrO_2 (80). Each of these materials also contains a higher temperature component centered near 573 K. The similarity in the H/D exchange profiles for these three samples paralles the similarity in the distribution of OH groups observed in the infrared spectra of these samples (see Fig. 6). Even higher peak temperatures for H/D exchange are observed for t-ZrO_2 (187) and am-ZrO_2 (325). Here too the distributions of OH group types on the surface of these samples bear some similarity.

Carbon dioxide, a weak acid, is known to adsorb on ZrO_2 in the form of both carbonate and bicabonate species [39,40,47–51]. Carbonate structures are formed via interaction of one or more of the of the oxygen atoms in CO_2 with zirconium cations in the lattice, as well as, with a surface oxygen atom, whereas bicarbonate structures are formed via the interaction of CO_2 with hydroxyl groups. Fig. 8 shows infrared spectra of adsorbed CO_2. The observed bands are assigned to either bidentate bicarbonate (1225, 1450, and 1625 cm^{-1}), b-HCO_3; bidentate carbonate (1325, 1335, 1498, 1556, and 1604 cm^{-1}), b-CO_3; or polydentate carbonate (1420 and 1450 cm^{-1}), p-CO_3; species in accordance with previously published studies [39,40,47–51]. The intensity of the band at 1225 cm^{-1} for b-HCO_3 per unit surface area is plotted in Fig. 9 versus the surface concentration of OH groups. Assuming that the absorption coefficient for the band at 1225 cm^{-1} is sample independent, the upward curvature of the plot in Fig. 9 indicates that the fraction of surface hydroxyl groups adsorbing CO_2 as b-HCO_3 is significantly higher for m-ZrO_2 (19 and 110) than t-ZrO_2 (187). This may be due to the higher fraction of tribridged OH groups on m-ZrO_2 samples. It is also notable that t-ZrO_2 (20) does not adsorb CO_2 as b-HCO_3, even though it has a reasonable surface concentration of OH groups, all of which are bibridged. This may be due to the weak basicity of these groups. Fig. 9 shows a plot of the total amount of CO_2 adsorbed per unit surface area based upon TPD measurements. Here again, there is a positive correlation between the total amount of CO_2 adsorbed per unit surface area and the surface concetration of OH groups. The principal difference between this plot and that presented in Fig. 9 is the curvature. This difference is attributed to the adsorption of CO_2 as b-CO_3 and p-CO_3, preferentially when the surface concentration of OH groups is small. Consistent with

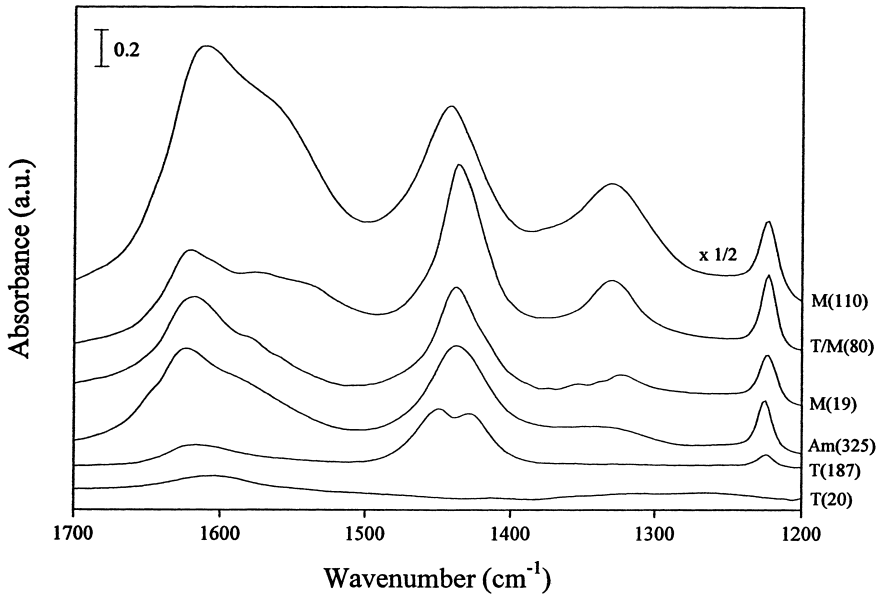

Fig. 8. Infrared spectra taken after exposure of zirconia to 0.16 MPa of CO_2 at room temperature. Each sample is identified as X (*Y*), where X = Am, T, T/M, or M and *Y* designates the BET surface area in m^2/g.

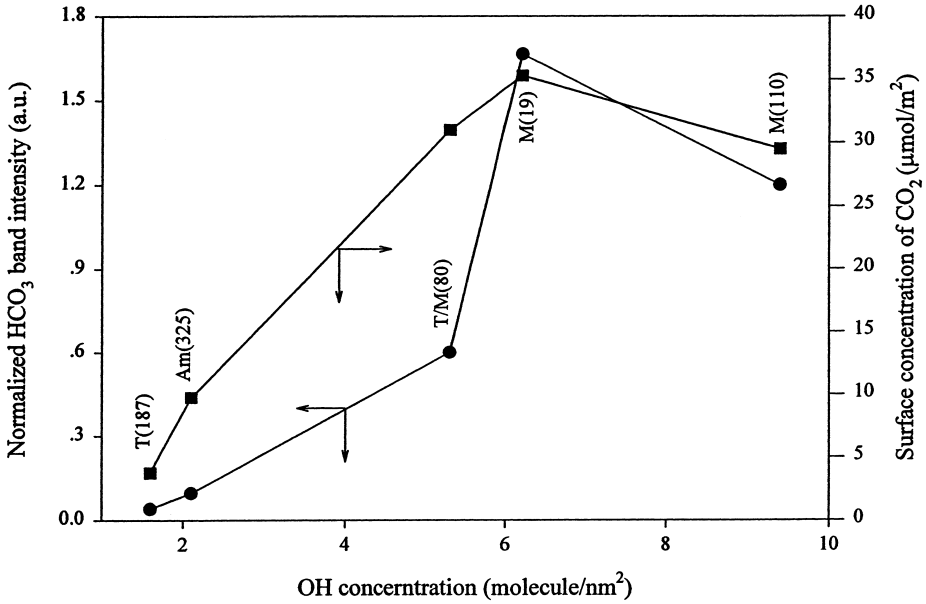

Fig. 9. Effect of hydroxyl surface concentration on the absorbance of the HCO_3 band at 1225 cm^{-1} divided by the BET surface area. Each sample is identified as X (*Y*), where X = Am, T, T/M, or M and *Y* designates the BET surface area in m^2/g.

this interpretation, the proportion of CO_3 to HCO_3 is seen to be significantly higher for t-ZrO_2 (187) than for m-ZrO_2 (110). Here again, it is notable that t-ZrO_2 (20) does not adsorb CO_2. The reason for this is believed to be a consequence of the weak Lewis acidity of Zr^{4+} cations and the corresponding weak Lewis basicity of O^{2-} anions present at the surface of this sample.

Consistent with the present findings, it has been reported that m-ZO_2 has stronger adsorption sites for CO_2 than those occurring on t-ZrO_2 [51]. It is suggested that the stronger adsorption sites due to increased basicity of Zr^{4+}–O^{2-} pairs.

Carbon monoxide, a weak base, can interact with either the Lewis acidic Zr cations or the Bronsted acidic hydroxyl groups present at the surface of ZrO_2 [14,15,38–46]. Fig. 10 shows infrared spectra for CO adsorbed as formate species (1569–1570 cm^{-1}), HCOO on each sample, and the corresponding loss of intensity in the OH portion of the spectrum. The assignment of the peaks associated with HCOO is based on the literature [14,15,38–46]. Fig. 11 demonstrates that there is a positive correlation between the amount of CO adsorbed as HCOO and the surface concentration of OH groups. As in the case of CO_2 adsorption, the fraction of OH groups reacting to form HCOO is higher for the m- than t-ZrO_2 (187), suggesting that the OH groups on m-ZrO_2 are more acidic.

Infrared spectra of molecularly adsorbed CO are shown in Fig. 12. The positions of these bands are reported in Table 2 together with similar results taken from the literature. With the exception of t-ZrO_2 (20), all of samples exhibit a peak for adsorbed CO for which the vibrational frequency of the C–O bond is above that for gaseous CO, 2143 cm^{-1}. The position of the CO band observed for t-ZrO_2 (187) is very similar to that reported previously [38,41,43–45]. Two overlapping bands centered at 2196–2192 and 2184–2182 cm^{-1} have been reported for CO adsorbed on m-ZrO_2. The first of these features is associated with defects in the ZrO_2 particles and the latter with adsorption sites located on the particle surfaces. The observation of only a single band at 2185 cm^{-1} in the present work suggests that relatively few defects are present. The position of the bands in all cases is characteristic of a simple σ-dative bond between adsorbed CO and a Zr^{4+} cation. Back donation of charge into the π^* orbital of CO is prevented by the d^0 nature of the cation, and hence the C–O vibrational frequency is blue-shifted relative to gas phase CO [41]. The extent of the shift in the vibrational frequency of adsorbed CO from 2143 cm^{-1} is a measure of the ability of the cation to σ-coordinate CO, i.e. Lewis acidity. In accordance with this interpretation, the observed trend in the values of $\Delta\nu$ indicates that the Lewis acidity increases in the sequence t-, m-ZrO_2 (80) < m-ZrO_2 (19) < am-ZrO_2 (325) < t-ZrO_2 (187). The anomalous sample is t-ZrO_2 (20) which exhibits and unexpectedly low value for $\Delta\nu$, as well as, a second peak for adsorbed CO that has a band located at 2109 cm^{-1}, which is below the frequency for gas phase CO.

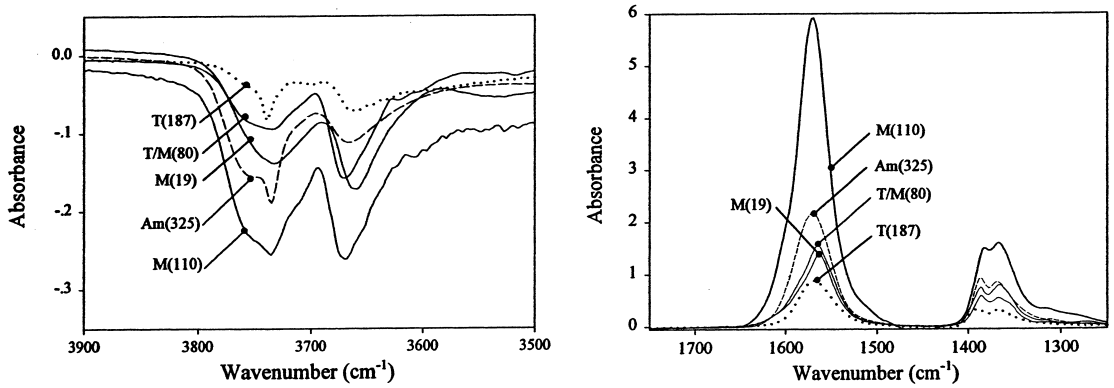

Fig. 10. Infrared spectra taken after exposure of zirconia to 0.16 MPa of CO at 523 K. The spectra show the formation of formate species and the corresponding loss of hydroxyl groups. Each sample is identified as X (*Y*), where X = Am, T, T/M, or M and *Y* designates the BET surface area in m^2/g.

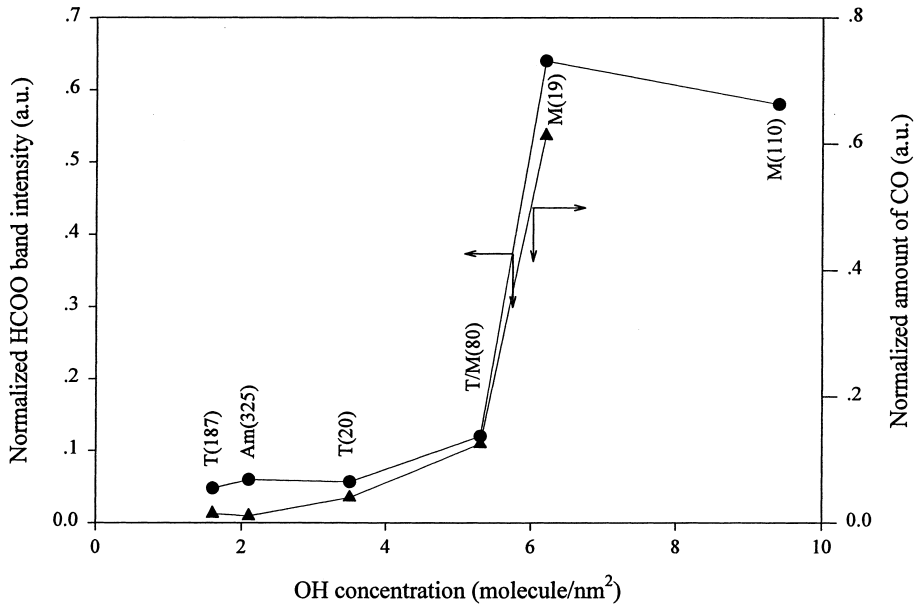

Fig. 11. Effect of hydroxyl surface concentration on the absorbances of CO and HCOO divided by the BET surface area. Each sample is identified as X (*Y*), where X = Am, T, T/M, or M and *Y* designates the BET surface area in m^2/g.

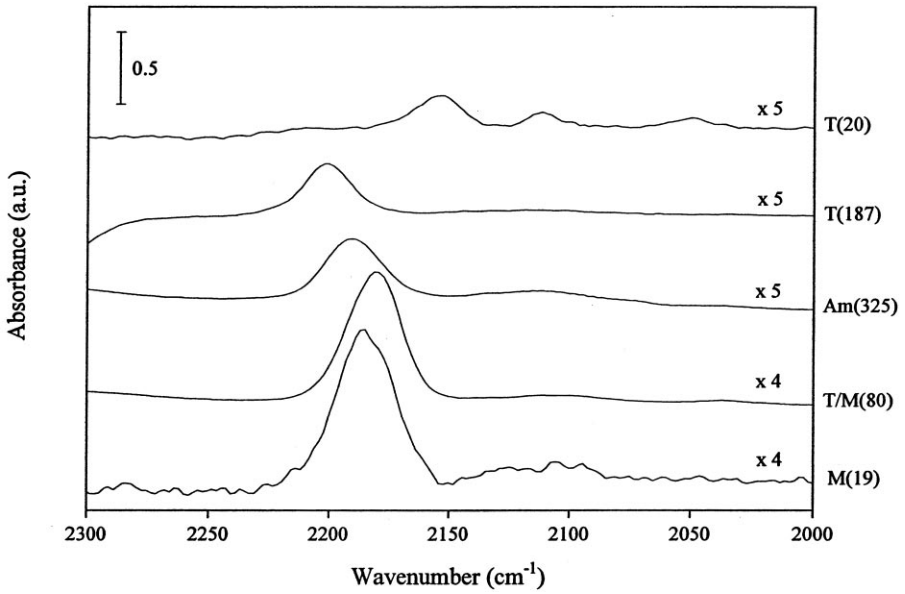

Fig. 12. Infrared spectra of molecularly adsorbed CO observed after exposure of zirconia to 0.16 Pa of CO at 523 K. Each sample is identified as X (*Y*), where X = Am, T, TIM, or M and *Y* designates the BET surface area in m^2/g.

Table 2
The position of vibrational frequency of the C–O and shift from gaseous CO

Sample	Wave number (cm^{-1})	ν (CO) shift from 2143 cm^{-1}	Full width at half maximum
Am (320)	2190.7	47.7	27.5
T (187)	2200.4	57.4	22.2
M (19)	2184.9	41.9	26.4
T/M (80)	2181.1	38.1	28.0
T (20)	2153.9	10.9	19.0

The intensity of the band for adsorbed CO plotted versus the surface concentration of OH groups is presented in Fig. 11. The trend in this quantity is virtually identical to that seen in the plot of the intensity of the band for HCOO species, strongly suggesting that there is a correlation between the two quantities. Surprisingly, the trend in the amount of CO adsorbed per unit surface area is opposite to the trend in $\Delta\nu$, which is usually viewed as a measure of the strength of CO interaction with Zr^{4+} cations, i.e. the Lewis acidity of the cations. This apparent inconsistency can be resolved on the basis of the model for CO interaction with the surface of ZrO_2 shown in Fig. 13. CO is envisioned to adsorb in two forms. The first involves adsorption at coordinatively unsaturated (cus) Zr^{4+} cations which are bonded to O^{2-} anions, none of which are associated with a proton, and the second involves adsorption at cus Zr^{4+} cations which are bonded to O^{2-} anions, one or more of which are associated with protons. It is expected that in the latter case the Lewis acidity of the Zr^{4+} cation will be lower, and consequently so will the value of $\Delta\nu$. The higher strength of adsorption may come from an interaction between the proton associated with a bridging hydroxyl group and the O atom of the adsorbed CO (see Fig. 13). Such an interaction would be conducive to the formation of an

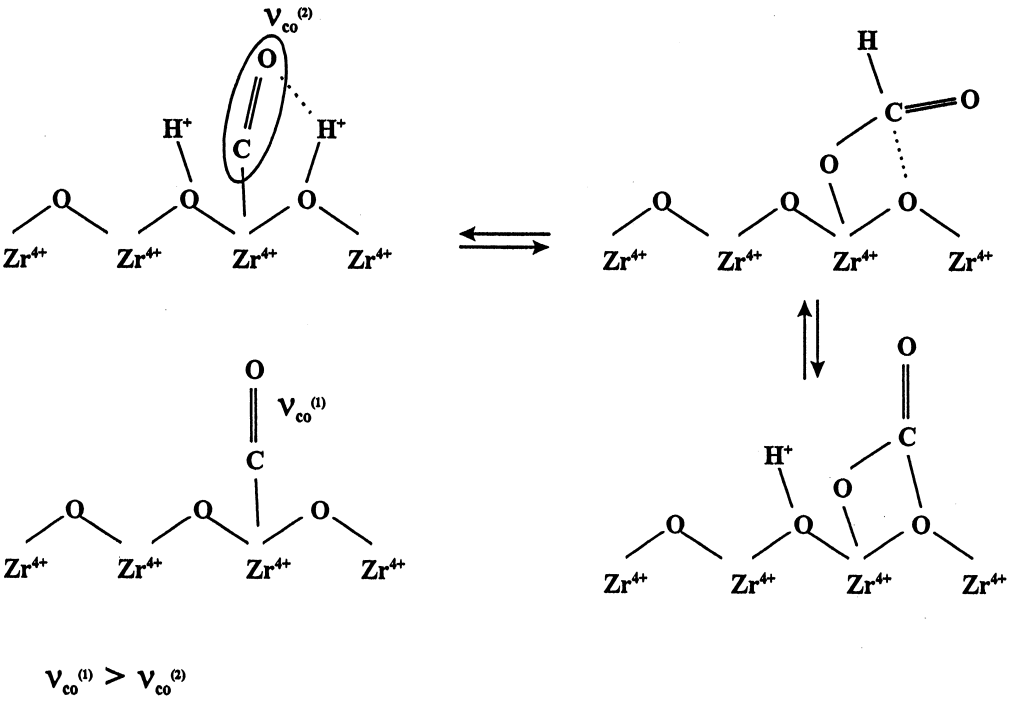

Fig. 13. Proposed model for the interactions of CO with the surface of zirconia.

HCOO group via the process shown in Fig. 13. This scheme could explain why there is a correlation between the amount of CO adsorbed as CO and HCOO, and why these quantities increase with increasing surface concentration of OH groups.

4. Conclusions

The conditions of synthesis, digestion, and calcination affect the phase, particle size, and surface area of ZrO_2 prepared from zirconyl chloride. Precipitation of ZrO_2 at high pH = 10 produces am-ZrO_2 with a surface area of 280 m^2/g. Extended digestion of this material at ambient pressure in NH_4OH increases its surface area to 400 m^2/g with no change in the ZrO_2 phase. Digestion in NH_4OH at elevated pressure (∼3 atm) decreases the surface area of the initially precipitated material to 200 m^2/g and brings about a nearly complete crystallization of the ZrO_2 to a mixture of t- and m-ZrO_2. Pricipitation of ZrO_2 at pH <1.5 leads to m-ZrO_2 with a surface area of 110 m^2/g. Calcination of the initially prepared ZrO_2 induces the transformation of am- to t-ZrO_2 and the transformation of t- to m-ZrO_2. A concurrent loss in surface area and a decrease in particle size are observed. The threshold for the tetragonal-to-monoclinic phase transformation is dictated largely by thermodynamic consideration in accord with the theory of Garvie and co-workers [55–59].

The surface properties of ZrO_2 are found to be a function of its bulk properties. The surface concentration of OH groups is highest on m-ZrO_2 and smallest on t-ZrO_2. Tribridged OH groups predominate on m-ZrO_2, whereas bibridged OH groups predominate on t-ZrO_2. The adsorption of CO_2 as HCO_3 per unit BET surface area increases with increasing surface concentration of OH groups. A similar trend is observed for the adsorption of CO as both CO and HCOO. This trend is attributed to the role of surface OH groups in stabilizing the adsorption of CO and the formation of HCOO.

Acknowledgements

The authors would like to express their appreciation to Professor Yong-Gun Shul of Yonsei University in Korea for helpful discussions. This work was supported by the Director, Office of Science, Chemical Sciences Division, U.S. Department of Energy under Contract DE-AC03-76SF00098.

References

[1] T. Yamaguchi, J. Hightower, J. Am. Chem. Soc. 99 (1977) 4201.
[2] Y. Tanaka, H. Hattori, K. Tanabe, Bull. Chem. Soc. Jpn. 51 (1978) 3641.
[3] Y. Nakano, T. Yamaguchi, K. Tanabe, J. Catal. 80 (1983) 307.
[4] R. Bird, C. Kemball, H.F. Leach, J. Chem. Soc., Faraday Trans. 1 (1987) 3069.
[5] Y. Nakano, T. Iizuka, H. Hattori, K. Tanabe, J. Catal. 57 (1979) 1.
[6] K. Arata, S. Akutagawa, K. Tanabe, Bull. Chem. Soc. Jpn. 49 (1976) 390.
[7] K. Arata, K. Kato, K. Tanabe, Bull. Chem. Soc. Jpn. 49 (1976) 563.
[8] T. Yamaguchi, H. Sasaki, K. Tanabe, Chem. Lett. 1017 (1973).
[9] B.H. Davis, P. Ganesan, Ind. Eng. Chem. Prod. Res. Dev. 18 (1979) 191.
[10] L. Bruce, J.F. Mathews, Appl. Cata1. 4 (1982) 353.
[11] L. Bruce, G.J. Hope, J.F. Mathews, Appl. Catal. 8 (1983) 349.
[12] Y. Amenomiya, Appl. Catal. 30 (1987) 57.
[13] B. Denise, R.P.A. Sneedon, Appl. Catal. 28 (1986) 235.
[14] I. Fisher, A.T. Bell, J. Catal. 172 (1997) 222.
[15] I. Fisher, A.T. Bell, J. Catal. 178 (1998) 153.
[16] D. Hamon, M. Vrinat, M. Breysse, B. Durand, M. Jebrouni, M. Roubin, P. Magnoux, T. des Courieres, Catal. Today 10 (1991) 613.
[17] R. Srinivasan, B.H. Davis, O.B. Cavin, C.R. Hubbard, J. Am. Ceram. Soc. 75 (1992) 1217.
[18] D.A. Ward, E.I. Ko, Chem. Mater. 5 (1993) 956.
[19] A. Clearfield, G.P.D. Serrette, A.H. Khazi-Syed, Catal. Today 20 (1994) 295.
[20] A. Coma, V. Fornes, M.I. Uan-adel, J.M. Lopez Nieto, Appl. Catal. A: Gen. 116 (1994) 151.
[21] M. Inoue, H. Koninami, T. Inui, Appl. Catal. A: Gen. 121 (1995) L1.
[22] A.F. Bedilo, K.J. Klabunde, NanoStruc. Matl. 8 (1997) 119.
[23] D.E. Collins, K.J. Bowman, J. Mater. Res. 13 (1997) 1230.
[24] Z. Zhan, H.C. Zeng, J. Mater. Res. 13 (1997) 2174.
[25] W. Stichert, F. Schuth, Chem. Mater. 10 (1998) 2020.
[26] G.K. Chuah, S. Jaenicke, B.K. Pong, J. Catal. 175 (1998) 80.
[27] G.K. Chuah, Catal. Today 49 (1999) 131.
[28] P. Afanasiev, A. Thiollier, M. Breysse, J.L. Dubois, Topics Catal. 8 (1999) 147.
[29] D.G. Barton, S.L. Soled, G.D. Meitzner, G.A. Fuentes, B. Iglesia, J. Catal. 181 (1999) 57.
[30] N.E. Tret'yakov, D.V. Pozdnyakov, O.M. Oranskaya, V.N. Filimonov, Russ. J. Chem. 44 (1970) 596.
[31] A.A. Tsyganenko, V.N. Filimonov, J. Mol. Struct. 19 (1973) 579.

[32] P.A. Agron, E.L. Fuller, H.F. Holmes, J. Colloid Interface Sci. 52 (1975) 553.
[33] T. Yamaguchi, Y. Nakano, T. Iizuka, K. Tanabe, Chem. Lett. 677 (1976).
[34] T. Yamaguchi, Y. Nakano, K. Tanabe, Bull. Chem. Soc. Japan 51 (1978) 2482.
[35] M. Benestil, V. Moravek, J. Lamotte, O. Saur, J.C. Lavalley, Spectrochim. Acta, Part A 43 (1987) 1487.
[36] J. Kondo, K. Domen, K. Maruya, T. Onishi, Chem. Phys. Lett. 188 (1990) 443.
[37] G. Cerrato, S. Bordiga, S. Barbera, C. Morterra, Appl. Surf. Sci. 115 (1997) 53.
[38] G. Cerrato, S. Bordiga, S. Barbera, C. Morterra, Surf. Sci. 50 (1997) 50.
[39] M.-Y. He, J.G. Ekerdt, J. Catal. 87 (1984) 381.
[40] W. Hertl, Langmuir 5 (1989) 96.
[41] C. Morterra, E. Giamello, L. Orio, M. Volante, J. Phys. Chem. 94 (1990) 3111.
[42] E. Guglielminotti, Langmuir 6 (1990) 1455.
[43] V. Bolis, C. Morterra, M. Volante, L. Orio, B. Fubini, Langmuir 6 (1990) 695.
[44] C. Morterra, V. Bolis, B. Fubini, L. Orio, T.B. Williams, Surf. Sci. 251/252 (1991) 540.
[45] V. Bolis, C. Morterra, B. Fubini, P. Ugliengo, E. Garrone, Langmuir 9 (1993) 1521.
[46] V. Bolis, G. Cerrato, Magnacca, C. Morterra, Thermochim. Acta 312 (1998) 63.
[47] Y. Nakano, T. Iizuka, H. Hattori, K. Tanabe, J. Catal. 57 (1978) 1.
[48] B.Q. Xu, T. Yamaguchi, K. Tanabe, Chem. Lett. 1663 (1988).
[49] J. Kondo, H. Abe, Y. Sakata, K. Maruya, K. Domen, T. Onishi, J. Chem. Soc., Faraday Trans. 84 (1) (1989) 511.
[50] C. Morterra, L. Orio, Mater. Chem. Phys. 24 (1990) 247.
[51] B. Bachiller-Baez, I. Rodriquez-Ramos, A. Guerrero-Ruiz, Langmuir 14 (1998) 3556.
[52] H. Toraya, M. Yashmura, S. Smiyama, J. Am. Ceram. Soc. 67 (1984) C-119.
[53] R. Cypres, R. Wollast, J. Roucq, Ber. Dent Keram. Ges. 40 (1963) 527.
[54] R. Garvie, J. Phys. Chem. 69 (1965) 1238.
[55] R. Garvie, J. Phys. Chem. 82 (1978) 218.
[56] R.C. Garvie, M.V. Swain, J. Mater. Sci. 20 (1985) 1193.
[57] R.C. Garvie, M.V. Swain, J. Mater. Sci. 20 (1985) 3479.
[58] R.C. Garvie, M.F. Goss, J. Mater. Sci. 21 (1986) 1253.
[59] R.C. Garvie, S.-K. Chan, Physica B 150 (1988) 203.